



A Fast Fermi Acceleration at Mars Bow Shock

K. Meziane, C. X. Mazelle, D. L. Mitchell, A. M. Hamza, E. Penou, B. M. Jakosky

► To cite this version:

K. Meziane, C. X. Mazelle, D. L. Mitchell, A. M. Hamza, E. Penou, et al.. A Fast Fermi Acceleration at Mars Bow Shock. *Journal of Geophysical Research Space Physics*, 2019, 124, pp.5528-5538. 10.1029/2019JA026614 . insu-03674429

HAL Id: insu-03674429

<https://insu.hal.science/insu-03674429>

Submitted on 20 May 2022

HAL is a multi-disciplinary open access archive for the deposit and dissemination of scientific research documents, whether they are published or not. The documents may come from teaching and research institutions in France or abroad, or from public or private research centers.

L'archive ouverte pluridisciplinaire **HAL**, est destinée au dépôt et à la diffusion de documents scientifiques de niveau recherche, publiés ou non, émanant des établissements d'enseignement et de recherche français ou étrangers, des laboratoires publics ou privés.

Copyright

JGR Space Physics

RESEARCH ARTICLE

10.1029/2019JA026614

Key Points:

- Flux spikes associated with sunward propagating energetic electrons observed upstream of the Martian bow shock
- Fast Fermi process operating at the foot of the Martian shock structure rather than the ramp
- Similarities and strong contrasts with the terrestrial foreshock

Correspondence to:

K. Meziane,
karim@unb.ca

Citation:

Meziane, K., Mazelle, C. X., Mitchell, D. L., Hamza, A. M., Penou, E., & Jakosky, B. M. (2019). A fast Fermi acceleration at Mars bow shock. *Journal of Geophysical Research: Space Physics*, 124, 5528–5538. <https://doi.org/10.1029/2019JA026614>





Received 13 FEB 2019

Accepted 7 JUN 2019

Accepted article online 2 JUL 2019

Published online 24 JUL 2019

A Fast Fermi Acceleration at Mars Bow Shock

K. Meziane^{1,2} , C. X. Mazelle² , D. L. Mitchell³ , A. M. Hamza¹, E. Penou²,
and B. M. Jakosky⁴ 

¹Physics Department, University of New Brunswick, Fredericton, New Brunswick, Canada, ²IRAP, Université de Toulouse, CNRS, UPS, CNES, Toulouse, France, ³Space Sciences Laboratory, University of California, Berkeley, CA, USA, ⁴Laboratory for Atmospheric and Space Physics, University of Colorado Boulder, Boulder, CO, USA

Abstract We report, for the first time, strong evidences that a fast Fermi mechanism is taking place at the Mars bow shock. The MAVEN spacecraft observations from the Solar Wind Electron Analyzer instrument show electron flux spikes with energies up to ~ 1.5 keV. These spikes are associated with sunward propagating electrons and appear when the interplanetary field line threading the spacecraft is connected near the Martian bow shock tangency point. The observed loss cone distribution is a salient feature of these backstreaming electrons as the phase space density peaks on a ring centered along the magnetic field direction. Moreover, the data show no evidence of any effect due to a hypothetical cross-shock electric potential on the observed angular distributions. Although similar distributions are seen at the terrestrial bow shock, the quantitative analysis of the measurements strongly indicates that the electrons are produced at the shock foot and escape upstream before exploring the entire shock structure.

1. Introduction

The Phobos-2 spacecraft reported for the first time the existence of energetic electrons upstream of the Martian bow shock (Skalsky et al., 1993a). Using the HARP differential electrostatic analyzer (Kiraly et al., 1991), Skalsky et al. (1993b) show that the electron flux is enhanced only when the field of view of the instrument and the magnetic field directions are nearly parallel. The authors interpreted these observations as a signature of the shock reflection of solar wind electrons. The Phobos-2 detector restricted field of view as well as a limited time measurement resolution provided an incomplete picture of the foreshock electrons.

Using a state-of-the-art instrumentation onboard of the MAVEN orbiter, a recent study from Meziane et al. (2017) revealed new insights of the Martian electron foreshock. An electron population emanating from the entire bow shock surface of Mars with energies reaching up to ~ 2 keV and having a flux intensity that is independent of shock geometry θ_{Bn} , the angle that the shock normal makes with the upstream ambient magnetic field, forms the main source of backstreaming electrons. This electron population exhibits a flux decrease with distance from the shock. This unexpected feature has been interpreted as the consequence of their impact with Martian exospheric hydrogen (Mazelle et al., 2018). The production mechanism at the shock remains to be elucidated, although the observed pitch angle distributions seem to indicate that electron reflection may be dominant. These findings somehow contrast with what is known in the terrestrial foreshock environment. A second foreshock electron population appearing as spikes with energies up to ~ 1.5 keV are detected when the interplanetary field line threading the spacecraft is connected near the Martian bow shock tangency point. These electron signatures are similar to analogous well-established observations in the terrestrial electron foreshock (Anderson et al., 1979). The present work focusses on this latter population.

Despite the lack of a global magnetic field, the existence of an induced magnetosphere produced by the interaction of the solar wind plasma with the planetary atmosphere and ionosphere implies the presence of the Martian bow shock, which has an impact on major upstream phenomena such as foreshock formation. Precisely, ions and electrons of solar origin, in addition to pickup ions, encounter the shock structure, which in turn modifies their complex trajectories, respectively. Moreover, the difference in plasma scale lengths as compared to the sizes of the Martian and Terrestrial obstacles suggests some fundamental dissimilarities between the solar wind interactions with the Martian bow shock and the Terrestrial foreshock, respectively. It is clear that the study of foreshock particle distributions will potentially shed some light on our understanding of important physical aspects of shock structure and its impact on downstream plasma

thermalization, a phenomenon poorly understood and in need of thorough investigation. In addition, particle reflection at the Martian shock still prevails and needs to be investigated thoroughly since the separation between quasi-parallel and quasi-perpendicular remains ill defined (Moses et al., 1988).

In the present report, quantitative arguments are developed to explain that the local acceleration of electrons at Mars results from a Fast Fermi process. According to our knowledge, although this may appear to be ordinarily associated with particle shock-related acceleration, this is the first time that such a phenomenon is reported in a planetary environment other than the terrestrial one. The observations are depicted in the next section, and a quantitative analysis is developed in section 3. Using an instructive parallel comparison with the terrestrial foreshock, a conclusion that summarizes the main results is presented in the last section.

2. Observations

The present study is based on observations from the MAVEN spacecraft, which currently is in orbit around Mars. The main objective of MAVEN's mission is to understand the physical mechanisms leading to the out-flow of volatile gas at Mars as a consequence of the solar radiation and the solar wind's interaction with the upper Martian atmosphere (Jakosky et al., 2015). The orbiter carries a state-of-the-art instrumentation able to fully accomplish the proposed science goals. In this study, we focus on data from the Solar Wind Electron Analyzer (SWEA) and the magnetometer (MAG). SWEA consists of a symmetrical hemispheric-shaped detector able to measure the energy and angular distributions of 3- to 4,600-eV electrons throughout the Martian environment (Mitchell et al., 2016). The instrument field of view spans 80% of all sky, and a half distribution function is obtained every 32 s, while the integrated flux is collected every 4 s near the shock, typically, the rate depending on altitude and Mars-Earth distance. The MAG sensors measure the vector magnetic field with a precision of ~ 0.35 nT with a sampling rate of 32 Hz (Connerney, Espley, Lawton, et al., 2015) and are designed to perform high-precision reliable measurements of the magnetic field in the Mars environment. The measurements' accuracy has been confirmed by the first results and compared with the electron pitch angle distribution in the solar wind (Connerney, Espley, DiBraccio, et al., 2015). In terms of time resolution, MAG provides, in the maximum high-telemetry mode, 32 vectors per second, sufficiently enough to study the dominant ion scale plasma processes occurring at the bow shock of Mars. In addition, solar wind ion plasma measurements are also used and these are from the Solar Wind Ion Analyzer (Halekas et al., 2015).

The time series of electron flux for 10 selected energy ranges is shown on the top panel of Figure 1 as recorded by MAVEN/SWEA on 4 January 2015 between 0230 and 0320 UT. The following successive panels display the magnetic field magnitude, the solar wind speed, the angle θ_{Bn} that the interplanetary magnetic field (IMF) makes with the local shock normal and the foreshock depth DIF , and the distance parallel to the X direction of the MAVEN position from the IMF tangent line to the shock, respectively. In the case where the magnetic field line is not connected to the shock, DIF is negative and the angle θ_{Bn} is not calculated. The remote determination of connection parameters, θ_{Bn} and DIF , necessitates the use of a model for the Martian bow shock surface; this shape has been investigated by several authors based on shock crossings identified in satellite data. All these models revolve around a fitting procedure that uses shock crossing locations to determine the best conic section. In all these available models, the conics' parameters are fixed and no adjustment to solar wind conditions is considered. In an aberrated solar ecliptic system, the Martian shock surface is usually represented in polar coordinates (r, θ) by

$$r = \frac{L}{1 + \epsilon \cos \theta} \quad (1)$$

In Mars Solar Orbital (MSO) system, the three parameters of the conics, the semilatus rectum L , the eccentricity ϵ , and the focus distance X_0 from the center of the planet, must be determined in order to fix the model. Based on expression (1), one approach to determine the triplet (L, ϵ, X_0) is to consider the function $F(L, \epsilon, X_0)$ given by the following form

$$F(L, \epsilon, X_0) = (X - X_0)^2 + Y^2 + Z^2 - (L - \epsilon(X - X_0))^2 \quad (2)$$

where (X, Y, Z) are the MSO coordinates of the spacecraft. The function F links the position of the MAVEN spacecraft with respect to the shock and at the time of the crossing $F(L, \epsilon, X_0) = 0$. An approximate solution

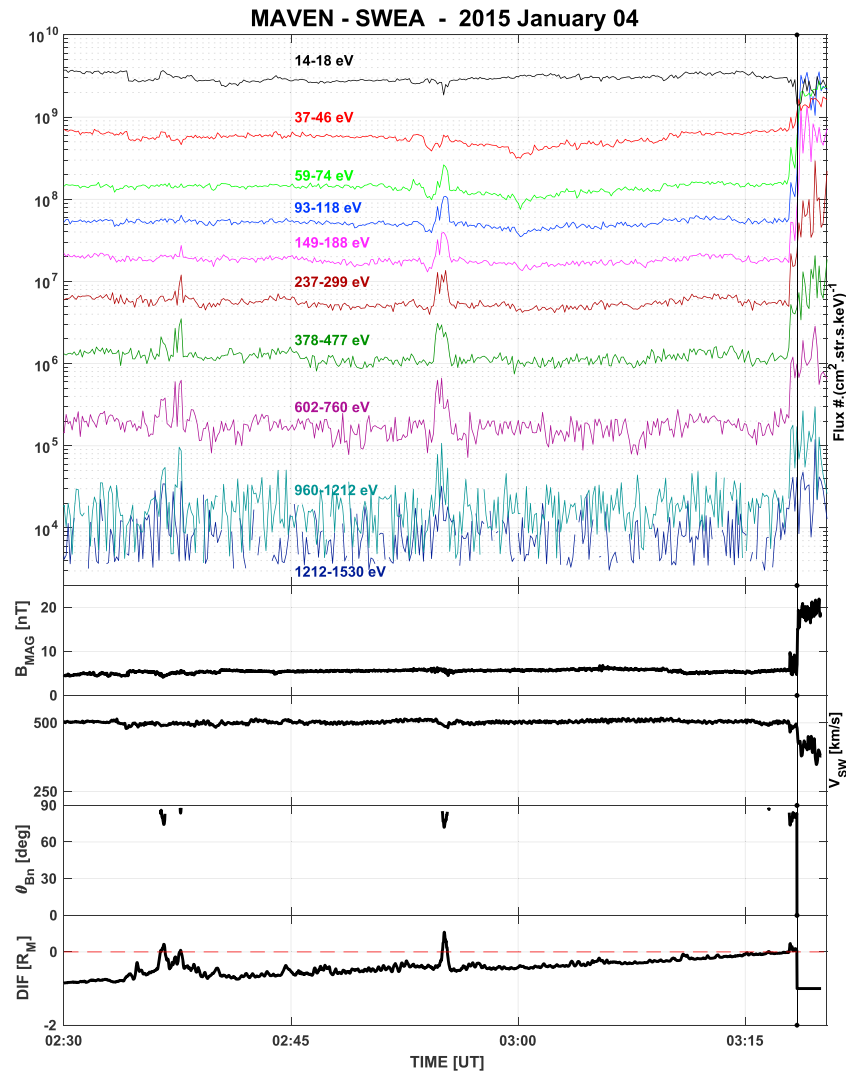


Figure 1. Top to bottom panels, respectively, show the electron flux for 10 selected energy ranges, the magnetic field magnitude, the solar wind speed, the shock θ_{Bn} , and the foreshock depth DIF for 4 January 2015 between 0230 and 0320 UT. MAVEN shock crossing is indicated by a thin vertical line at $\sim 0318:25$ UT. SWEA = Solar Wind Electron Analyzer.

for (L, ϵ, x_0) is obtained by minimizing $F(L, \epsilon, X_0)$ at the time of the Martian bow shock crossing by MAVEN, which occurs at 0318:25 UT. We found $L = 2.53R_M$ (Mars's Radius), $\epsilon = 1.03$, and $X_0 = 0.70R_M$. These numerical values can be compared with statistical models from Vignes et al. (2000; $L = 2.04R_M$, $\epsilon = 1.03$, $X_0 = 0.64R_M$), Trotignon et al. (1991; $L = 2.17R_M$, $\epsilon = 0.95$, $X_0 = 0.50R_M$), Slavin et al. (1991; $L = 2.07R_M$, $\epsilon = 1.01$, $X_0 = 0.55R_M$), or Schwingenschuh et al. (1990; $L = 2.72R_M$, $\epsilon = 0.85$, $X_0 = 0.0R_M$). During the time interval of Figure 1, all previously cited models point to a situation where the MAVEN spacecraft remains magnetically disconnected from the shock, which seems to be in agreement with the electron data since the fluxes for all energies are sustained to a constant level corresponding to solar wind electrons. However, none of these models captures the 0318:25 UT crossing. Moreover, the shock parameters derived from the minimization of expression (2) point at the fact that the IMF field lines threading the MAVEN spacecraft remain unconnected ($DIF < 0$) during the entire interval shown in Figure 1 except for two short durations that we examine next. The model, however, reproduces MAVEN's inbound crossing as indicated by the vertical line in DIF (or θ_{Bn}) plot, remarkably. Furthermore, Figure 1 shows short-lived/abrupt electron flux enhancements for $E \geq 37$ eV which peak at $\sim 0236:40$, $\sim 0237:45$, and $\sim 0255:00$ UT, respectively. It is important to note that the model bow shock used here captures the magnetic connection when the electron bursts are observed, indicating that the shock has not moved significantly. These electron bursts,

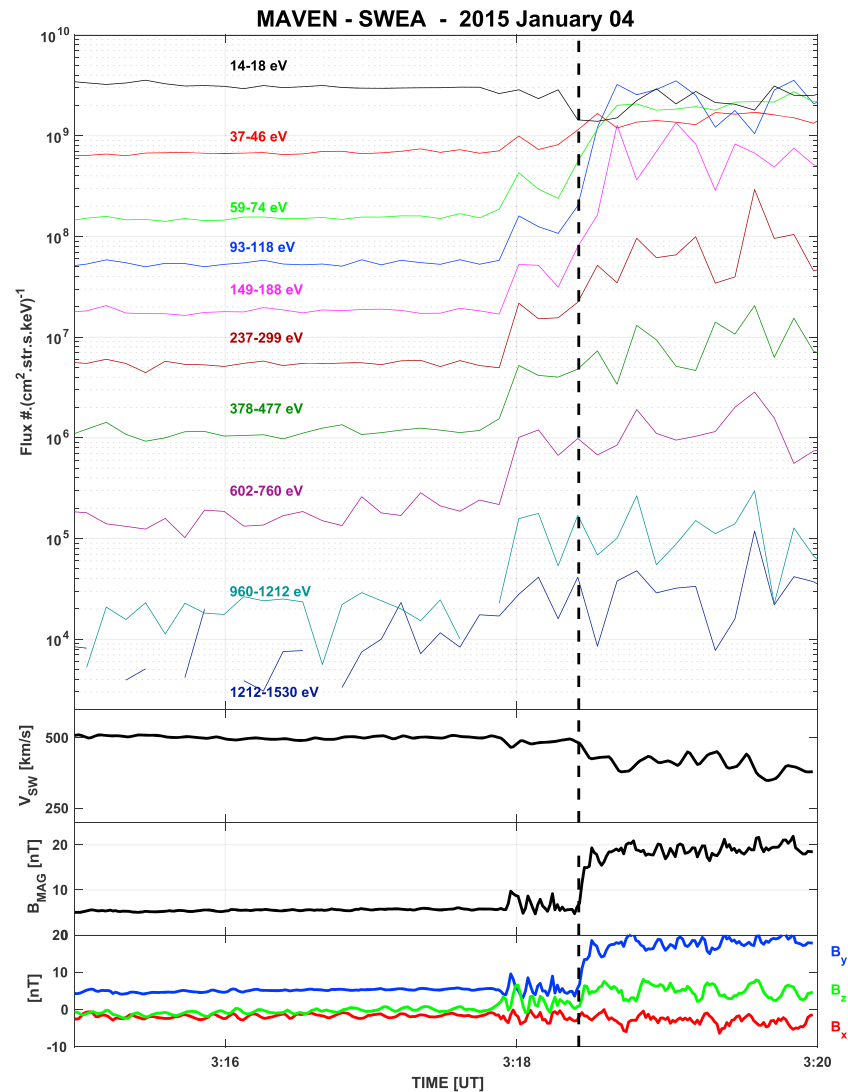


Figure 2. Top to bottom panels, respectively, show the electron flux for 10 selected energy ranges, the solar wind speed, the magnetic field magnitude, and the Mars Solar Orbital components of the magnetic field for 4 January 2015 between 0315 and 0320 UT. The vertical dashed line indicates the shock crossing. SWEA = Solar Wind Electron Analyzer.

as indicated in the *DIF* panel plot, appear in the SWEA analyzer due to a rapid back and forth change in the IMF direction, while the spacecraft remains clearly outside the foreshock ($DIF < 0$) grazing the shock-IMF tangent line; the short MAVEN intrusions in the foreshock are indicated by $DIF > 0$. Interestingly, it is worth noticing the association of the electron spectrum with the connection parameters. For the 0237:45 UT burst, the lower-energy threshold corresponds to $E \sim 74$ eV while it is lower for the 0255:00 UT burst ($E \sim 37$ eV), and at the same time MAVEN is located deeper in the foreshock for the latter when compared to the former.

The association of backstreaming electrons with the Martian bow shock prompts a scrutiny of the shock region. Figure 2 shows an enlargement of Figure 1 around the time of interest, between 0315 and 0320 UT in which the *DIF* and the θ_{Bn} panels have been replaced by time series representing the IMF MSO components. Before the shock ramp crossing, indicated by the dashed vertical line, Figure 2 clearly shows, starting at 0317:57 UT, a magnetic structure that is strongly similar to a foot commonly seen in front of quasi-perpendicular supercritical shocks. It is important to notice the electron flux enhancement, up to ~ 1.5 keV, when MAVEN happens to be inside the foot region. As we elaborate below, the existence of the magnetic foot at the shock front plays a determinant role in understanding the observed electron distribution functions.

04/Jan/2015 02:55:11.836

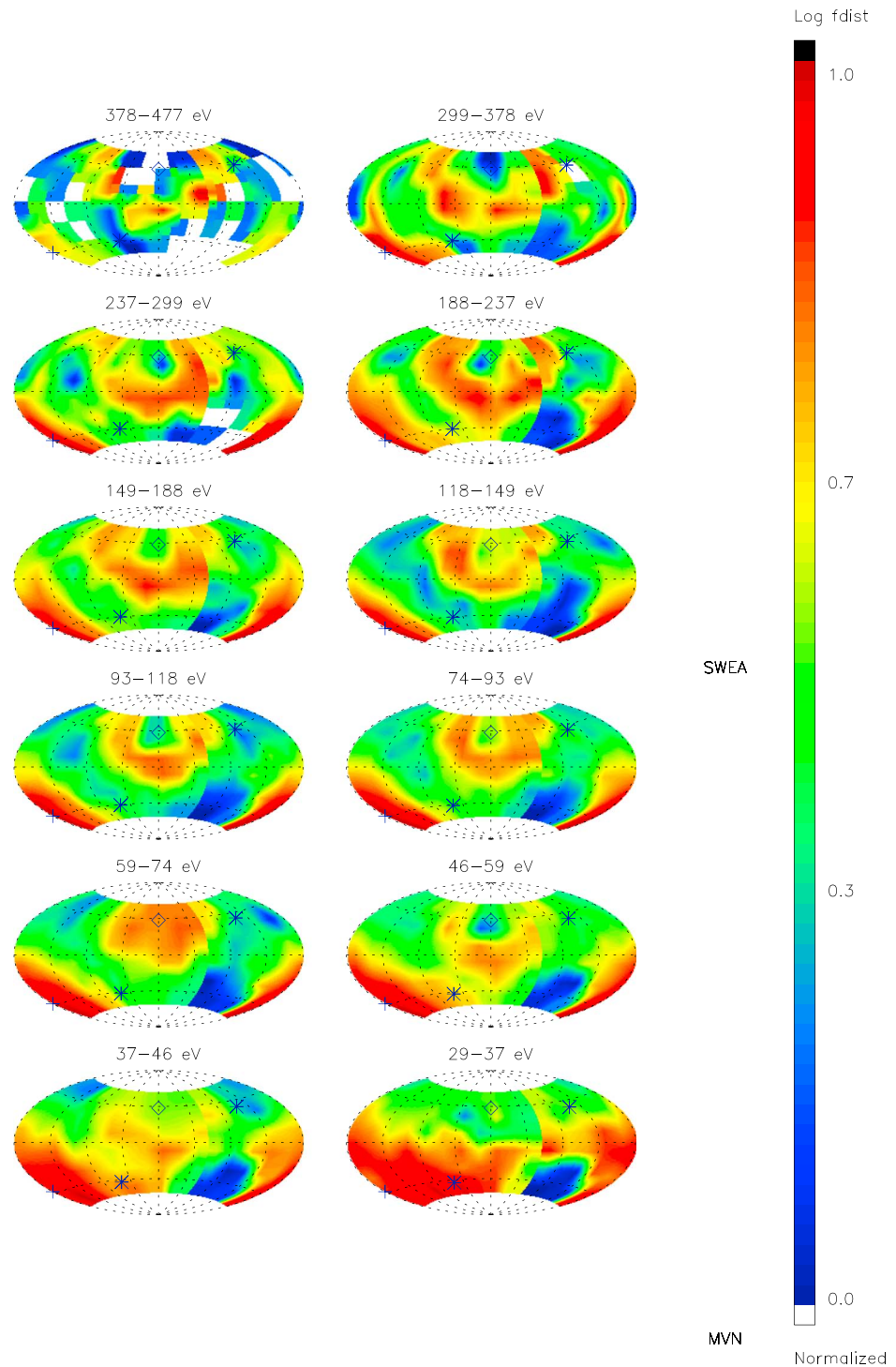


Figure 3. Snapshots of electron angular distribution for selected energy ranges taken at 0255:11 UT. The Hammer-Aitoff equal area projection is used. The “+” (“o”) symbol represents the direction of B ($-B$) direction. The color scale corresponds to distribution function values and is normalized for each Hammer-Aitoff slice.

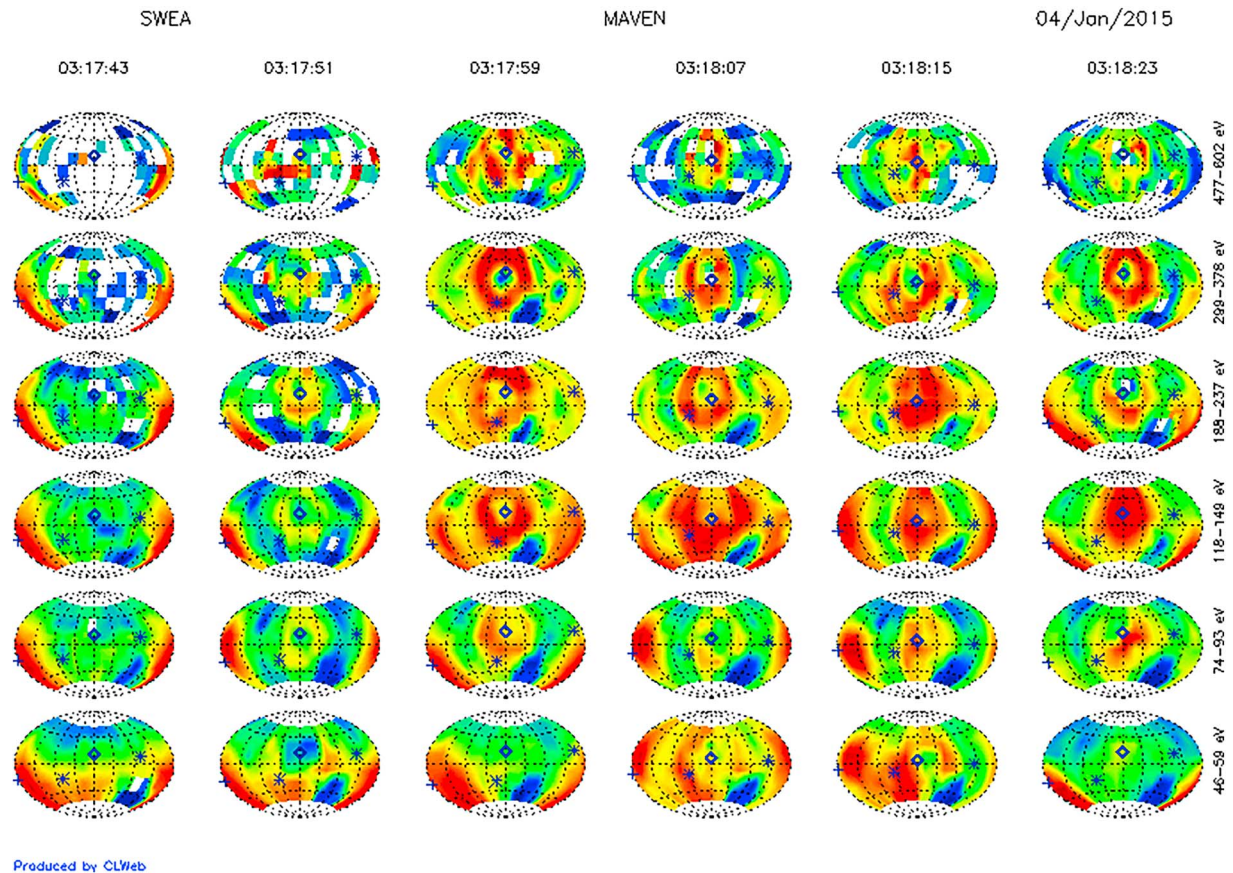


Figure 4. Snapshots of electron angular distribution for selected energy ranges taken between 0317:43 and 0318:07 UT. A similar format as in Figure 3 is used.

Pursuing further the observation, we now examine in detail the electron angular distribution. For this purpose, the Hammer-Aitoff equal area projection (Mailing, 1992) is used to represent three-dimensional measurements of electron distributions as shown in Figure 3. The projection is appropriate to display 4π steradians projections for a given energy and has been used with terrestrial foreshock electron observations (Larson et al., 1996) and ions (Meziane et al., 2001). Each slice is a representation in pitch angle (radial extent) gyrophase (polar angle) dimensions for a fixed energy. In this representation, field-aligned propagating particles show a space phase density peak centered on the “+” or “o” symbol (indicating the direction of B or $-B$, respectively). The blank polar sectors visible in each distribution are velocity space regions that are not covered by SWEA, while the asterisk symbol “*” shows the solar wind direction. During the time interval of interest, the magnetic field direction is planetward; the backstreaming particles are therefore primarily streaming in $-B$ direction indicated by the o symbol as shown on each Hammer-Aitoff slice. Figure 3 shows eight snapshots for 12 selected energy ranges as indicated on top of each slice. The solar wind strahl, a population of solar wind electrons (energies >40 eV at 1 AU) that propagate in beams parallel to the magnetic field direction (Feldman et al., 1975; Rosenbauer et al., 1977), is clearly identified in Figure 3 for energies $E > 74$ eV. It coincides with the IMF direction as indicated by the + symbol; its intensity decreases with energy. Figure 3 also depicts a nearly closed ring or annulus centered along the $-B$ direction and representing a peak in phase space density seen above $E > 37$ eV. In addition, it seems that the pitch angle (the ring radius) appears slightly larger for the electron energy channel $E = 378$ –477 eV than for $E = 188$ –237 eV and below, though for the highest-energy channel the ring is not well resolved.

In support of further analysis, the electron angular distribution recorded after the burst during the inbound MAVEN motion and precisely within the shock foot just before MAVEN shock crossing is shown in Figure 4; a similar format as in Figure 3 is used. Similar ring distributions are observed throughout the shock foot between 0317:52 and 0318:72 UT, and the ring structure disappears after the shock ramp. The ring can be clearly identified on energy channels starting from 46–59 up to 780–960 eV (not shown).

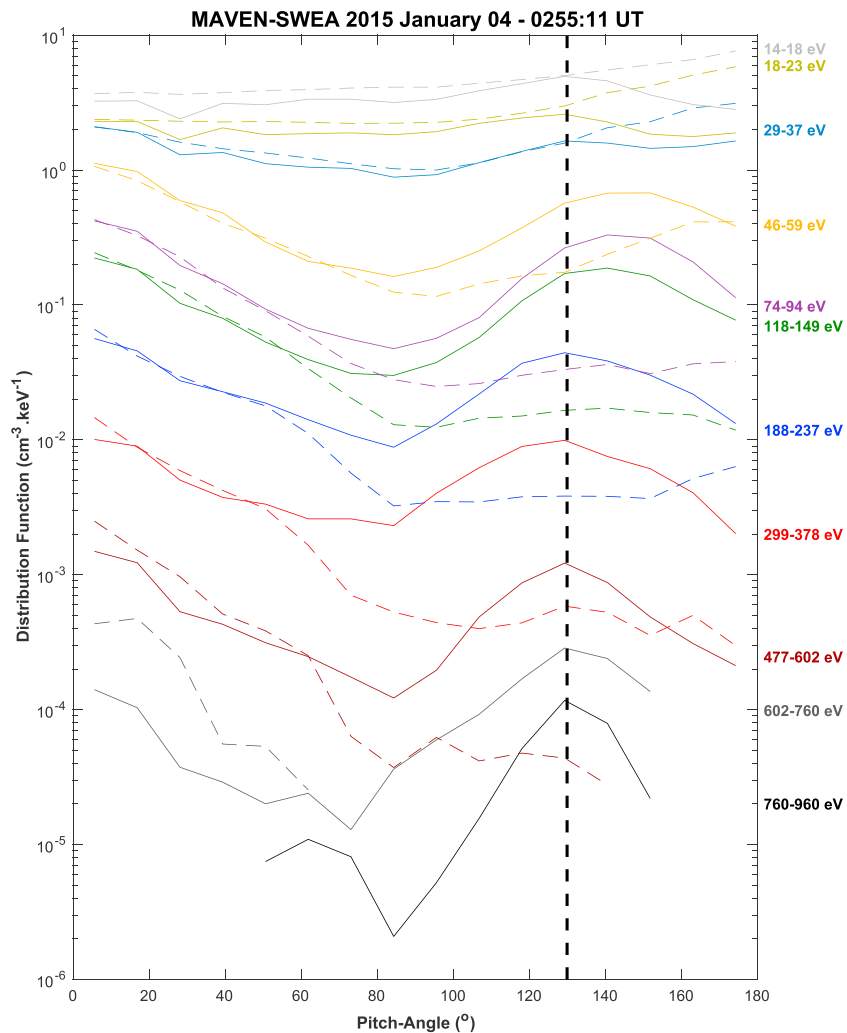


Figure 5. The continuous lines show the phase space density variation versus pitch angle for selected energy channels observed by MAVEN-SWEA analyzer on 4 January 2015, 0255:11 UT. The thin dashed lines correspond to the solar wind distribution taken 0253:59 UT for which MAVEN is not magnetically connected. The vertical line indicates a pitch angle of 130°. The energy ranges are indicated on the right of the figure.

3. Quantitative Analysis

From a quantitative standpoint, the continuous lines in Figure 5 show a more conventional representation of the pitch angle distribution. For the electron burst observed at 0255:11 UT, the distribution is sampled in the plasma rest frame and is retrieved from the 3-D angular distribution of Figure 3 and in which the integration over the gyrophase has been performed. In addition, the dashed lines in Figure 5 represent the solar wind pitch angle distribution measured at a not so distant instant (0253:59 UT) when MAVEN was outside the foreshock. Figure 5 clearly depicts the solar wind electron isotropic core (and part of the halo) ($E = 14\text{--}18\text{ eV}$) and the strahl ($E \geq 37\text{ eV}$). Both solar wind components clearly identified whether MAVEN is inside or outside the Martian foreshock. The electron spike is associated with a significant flux enhancement above the solar wind threshold and corresponds to sunward moving electrons (pitch angle $>90^\circ$). Clearly, the electron phase space density maximum is not aligned with the magnetic field direction. While $E \geq 149\text{ eV}$ electrons exhibit a peak at $\sim 130^\circ$, at lower energy ($E = 59\text{--}118\text{ eV}$) the phase space density values peak sensitively at higher pitch angle values ($\sim 150^\circ$). Due to a limited angular resolution of SWEA, the progressive decrease of the pitch angle from higher to lower electron energies is fairly noticeable (Meziane et al., 2017).

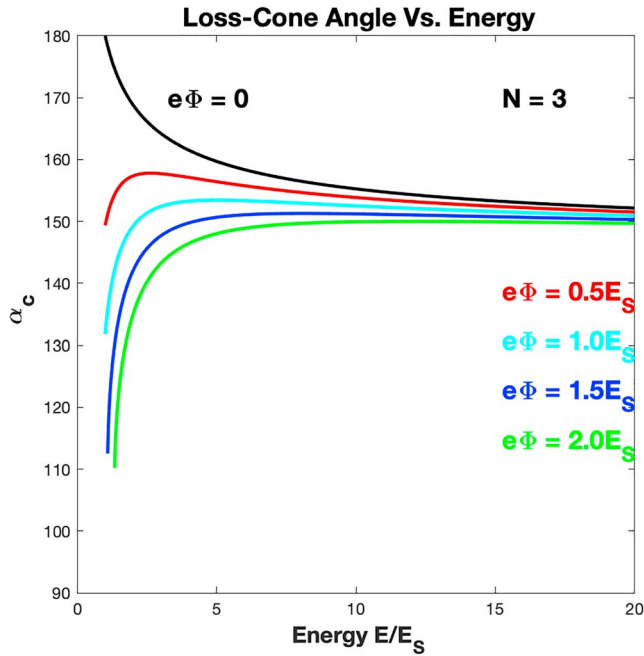


Figure 6. Mirror loss cone angle α_c versus electron energy for a magnetic ratio $N = 3$ for various cases based on $e\Phi$ values as indicated by the color of each curve.

The observations presented in the above section clearly point to similarities with the terrestrial foreshock. It is known that sheets of sunward propagating energetic electrons are always present on IMF field lines nearly tangent to the Earth bow shock (Anderson et al., 1979). The most energetic electrons emanate near the tangent line, whereas less energetic ones emerge from regions located relatively deep, downstream of the IMF tangent line. Therefore, the bursty appearance is due to the IMF line tangent to the bow shock sweeping the spacecraft. The occurrence of electron bursts at the Martian foreshock results in the same fashion as they are seen when the foreshock connection depth DIF nears zero. The analogy pinpoints to a similar physical mechanism, responsible for the electron energization, operating at both planetary shocks. In this context, the seminal works by Wu (1984) and Leroy and Mangeney (1984) are fundamentally relevant since they provide the theoretical framework for the production mechanism of electron bursts seen at planetary bow shocks. The theoretical models are based on an adiabatic reflection mechanism of a subpopulation of solar wind electrons by planetary bow shocks. In agreement with these models, a later work from Larson et al. (1996) provided strong observational evidence that a mirror reflection of a population of solar wind electrons takes place at the Earth's bow shock. In this latter study, based on WIND-3DP experiment, Larson et al. (1996) report that the distributions have a loss cone angle increasing with decreasing energy pinpointing the presence of a significant cross-shock potential affecting lower-energy reflected electrons. In the present study, no such effect is observed, and as explained below, the variation of the loss cone

angle with energy stipulates in fact that the adiabatic reflection of electrons occurs in a static electric potential-free space region.

Furthermore, the mirror loss cone angle α_c provides an unambiguous component for testing the theoretical models since it is precisely determined. For a quasi-parallel geometry, a simple approximate expression for α_c independent of the shock speed V_s can be obtained (Larson et al., 1996). However, for nearly perpendicular shocks, the approximation does not hold. Following Decker (1983), and making a readjustment to account for the cross-shock potential energy $e\Phi$, we can show (see the appendix) that the critical pitch angle α_c for an electron energy E is given by

$$\mu_c = \cos \alpha_c = \frac{1}{N} \left[\eta + \sqrt{(N-1)(N-\eta^2) - N\eta^2 \left(\frac{e\Phi}{E_s} \right)} \right] \quad (3)$$

with $N = B_M/B_1$ and $\eta^2 = E_s/E$, where B_1 and B_M are the magnetic field magnitude upstream and at the mirror point, respectively. To derive expression (3), a planar shock is assumed. As the Larmor radius of a typical solar wind electron is several orders of magnitude smaller than the curvature of the Mars's bow shock, the assumption is not violated.

In expression (3), all reflected electrons that escape upstream have an energy E larger than the critical energy $E_s = m_e V_s^2/2$, that is, $\eta \leq 1$. For fixed values of E_s and $e\Phi$, one can determine μ_c using expression (3) for different ranges of electron energy E and compression ratio N . For supercritical shocks, N may exceed by about 25% the MHD asymptotic value of $N = 4$. The theoretical prediction of μ_c requires knowledge of the parameters $e\Phi$ and E_s . The cross-shock electric potential Φ is inherent to supercritical shocks as it arises mainly from a combination of electron pressure gradients and the Hall current (Scudder et al., 1986). At the Earth's bow shock, the cross-shock potential energy in the deHoffmann-Teller frame may reach a significant fraction of the incident flow energy (up to $\sim 30\%$; Schwartz et al., 1988). Measurements suggest a tendency of the electric potential jump to decrease in magnitude with increasing Mach number. In terms of magnitude, the Mach number is slightly higher at Mars (Halekas, 2017). It is therefore expected that the cross-shock potential at Mars to be less in comparison to that of Earth but remains significant still. As a result, the incoming ions are repelled by the macroscopic electric field while the electron reflection is mitigated since electrons should overcome the cross-shock potential to escape upstream.

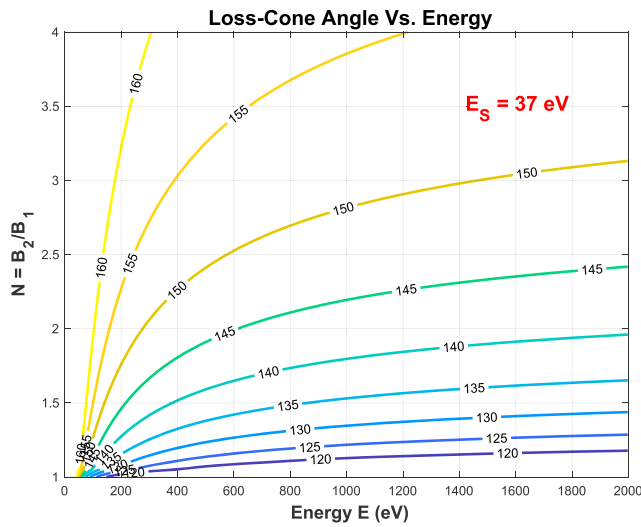


Figure 7. Left panel shows the contours that provide the mirror reflection loss cone angle α_c in degrees for a particle with energy E and shock ratio N ranges while the critical energy $E_S = 37$ eV and $e\Phi = 0$ eV.

Figure 6 depicts the effects of the cross-shock potential on electrons encountering the shock boundary. For illustration purposes, the particle energy and the shock potential energy are normalized to E_S and a shock compression ratio $N = 3$ is arbitrarily chosen. On the figure, the black continuous curve corresponds to $e\Phi = 0$ while the red, cyan, blue, and green curves correspond to the cases $e\Phi = 0.5E_S, E_S, 1.5E_S, 2E_S$, respectively. By analogy with the observations, $180^\circ - \alpha_c$ is plotted instead of α_c which given is by expression (3). While at high energy, the effect of the cross-shock potential on the loss cone tends to remain small, at low energy the variation of the loss cone (with energy) is reversed when the cross-shock potential is present. In comparison with the case $e\Phi = 0$, the effect on the loss cone is more important as the potential jump across the shock increases. In other terms, in the presence of a significant cross-shock potential, the loss-cone angle at high electron energy appears smaller when compared to the case of low-energy electrons. On the contrary, a reflection from a potential-free shock is considered, higher-energy escaping electrons require pitch angles that are larger than those of low-energy electrons (since the parallel velocity is relevant).

The determination of E_S requires more caution. The inspection of the electron distribution shown in Figure 5 also reveals sunward moving electron fluxes over the solar wind flux level only for energies larger than

~ 37 eV, which is consistent with the lack of electron bursts below this energy (Figure 1). The absence of $E \leq 37$ -eV flux enhancement may be due to two distinct factors. The burst occurrence at 0255:11 UT results from a small IMF rotation. In the situation where the shock θ_{Bn} remains larger than a threshold value, $E \leq 37$ -eV electrons cannot escape upstream; in this particular case, $E_S \sim 37$ eV. Another possibility is related to particle velocity filtering. Due to solar wind convection, thin sheet particle layers are not located in the same region of space, and therefore, all energies are not seen simultaneously. As a consequence, dispersed bursts in time should occur. The electron burst presents no evidence for any dispersion; however, it is likely that the time measurement resolution remains insufficient to catch a possible dispersion. For this particular situation, $E_S < 37$ eV. Finally, the numerical value of E_S could be estimated from the connection parameters derived from the bow shock model. We found that the 0255:11 UT electron burst occurs for $\theta_{Bn} \sim 84.5^\circ$ and $\theta_{vn} \sim 129^\circ$ the angle the direction of the plasma flow makes with the local shock normal. With a solar wind speed $V_{sw} \sim 495$ km/s, we found $E_S \sim 31$ eV in good agreement with the observed electron spectrum.

Maintaining a value of ~ 37 eV for the predicted critical energy E_S , the mirror angle $180^\circ - \alpha_c$ contours for a range of N and energy E are shown in Figure 7; the 180° offset is enforced because sunward moving electrons have pitch angles $> 90^\circ$. In Figure 7, $e\Phi = 0$ eV, and this choice is discussed below. One should emphasize that the analytical results of Figure 7 remain qualitatively unchanged for other possible values of $E_S < 37$ eV (not shown). Quantitatively, at the same time, the contour values slightly increase but remain insignificant in comparison with the angular resolution of the measurements.

It is reasonable to assume, under nominal solar wind conditions, that one is dealing with a supercritical quasi-perpendicular shock, as it is the case for the Martian bow shock crossing above (we estimated $M_{MS} \sim 3.7$), and the typical shock magnetic compression ratio N is larger than ~ 2 . For the present case event $N \sim 3.2$ and it reaches $N \sim 4$ if the overshoot is taken into account. It clearly appears from Figure 7 that typical shock magnetic compression ratios predict critical pitch angles significantly smaller than the observed ones. Precisely for $E = 760$ - to 960 -eV range, the observed critical pitch angle is accounted by a compression ratio $N \sim 1.3$. The agreement for the lower energies with a similar compression ratio cannot be dismissed. Moreover, a reflection from the shock ramp, where presumably a cross-shock potential must be significant, would result, as explained above and shown in Figure 6, noticeable signatures in the electron pitch angle distributions. Based on equation (3), we found an upper threshold for $e\Phi \sim 0.1E_S$ (or $e\Phi \sim 3.7$ eV). Such a value is of the same order as the expected spacecraft potential (not taken into account here since negligible for the energies considered). These results strongly suggest that the electrons do not explore the entire shock ramp and consequently the shock overshoot. As described in detail in section 2, from the instant where the spike is seen to the shock crossing, the time evolution of the connection depth DIF shown in Figure 1

indicates that MAVEN spacecraft remains in a grazing position with respect to the IMF tangent line. Before reaching the shock ramp, the spacecraft encounters a foot for which the maximum magnetic compression ratio B_M/B_1 is 1.5–1.6. The increase of the magnetic field magnitude inside the foot region is sufficient to prompt a reflection of incoming electrons, and the observed pitch angles are in good agreement with what is expected from a magnetic mirror reflection. Although the source region of the electron spike observed upstream cannot be determined precisely, the similarities of the associated angular distribution with the mirror reflected electrons at the foot are striking. This strongly suggests that the source region of the electron spike is very similar to the shock structure seen subsequently. At this point, a conclusive empirical determination can only be reached through higher time resolution electron measurements and a comprehensive understanding of the encounter of the solar wind electrons with the Martian bow shock demands a theoretical development that goes beyond the simple process emulated in expression (3).

4. Conclusion

In the present study, we report bursts of sunward propagating energetic electrons upstream of the Martian bow shock. These events are seen along IMF field lines that are nearly tangent to the Martian shock surface. The quantitative analysis of the electron pitch angle distribution demonstrates that the electron spikes are produced, like at the terrestrial bow shock, by a fast Fermi acceleration process. The present observations show for the first time that such a coherent process occurs at the Martian quasi-perpendicular shock. Nevertheless, an essential difference regarding the source region exists between Earth and Mars. While solar wind electrons explore the entire shock layer, including the overshoot, before getting reflected upstream of the Earth's bow shock, they can bounce back at the shock foot in the Martian case and not necessarily at the ramp or the overshoot. This distinction needs to be investigated as the Martian shock structure remains to be fully understood.

Appendix A: Rest Frame Pitch Angle of a Particle After Its Encounter With a Shock

In the presence of an electric potential Φ' in region where a gradient of a magnetic field exists, the pitch angle α' of an electron cannot be less than α'_c , where after (Fitzenreiter et al., 1990; Leroy & Mangeney, 1984)

$$\sin^2 \alpha'_c = \frac{B_1}{B_M} \left(1 + \frac{e\Phi'}{E'} \right) \quad (\text{A1})$$

In the context of a shock wave, E' , α'_c , and $e\Phi'$ are, respectively, the particle kinetic energy, the critical pitch angle, and the electric potential energy expressed in deHoffmann-Teller reference frame; B_1 and B_M are the magnetic field magnitude upstream and at the mirror point. Setting $N = \frac{B_M}{B_1}$ and $\mu'_c = \cos \alpha'_c$ yields

$$\mu'_c = \sqrt{1 - \frac{1}{N} \left(1 - \frac{e\Phi'/E'}{N-1} \right)} \quad (\text{A2})$$

Clearly from above, the presence of a cross-shock potential implies a larger cone angle comparatively to the case $e\Phi' = 0$. Now, one needs to write the last equation in the plasma rest frame. If E and μ_c are the particle energy and the cosine of the critical pitch angle given in the plasma rest frame, the transformation from deHoffmann-Teller frame provides (Decker, 1983)

$$\frac{E'}{E} = 1 - 2\eta\mu_c + \eta^2 \quad \text{and} \quad \mu'_c = \frac{\mu_c - \eta}{\sqrt{1 - 2\eta\mu_c + \eta^2}} \quad (\text{A3})$$

where $\eta^2 = \frac{E_S}{E}$ with E_S the kinetic energy associated with the shock speed V_S ; only reflected particles with $\eta \leq 1$ can escape upstream. Since the reference frame transformation is only parallel to the magnetic field direction, a Galilean transformation leaves the electric field unchanged: $\Phi = \Phi'$. The critical pitch angle μ_c is now derived after eliminating E' , Φ' , and μ'_c from expression (A2). We obtain

$$\mu_c = \cos \alpha_c = \frac{1}{N} \left[\eta + \sqrt{(N-1)(N-\eta^2) - N\eta^2 \left(\frac{e\Phi}{E_S} \right)} \right] \quad (\text{A4})$$

which is expression 3eq. Above equation shows that a minimum value for μ_c exists at particle energy E such that

$$\eta^2 = \frac{1}{2} \frac{N(N-1)}{N-1-N(e\Phi/E_S)} \quad (\text{A5})$$

Acknowledgments

MAVEN data are publicly available through the Planetary Data System. This work is supported by the French space agency CNES for the observations obtained with the SWEA instrument. Work at UNB is supported by the Canadian Natural Science and Engineering Council. MAVEN data are publicly available through the Planetary Data System (<https://pds-ppi.igpp.ucla.edu/>).

References

- Anderson, K. A., Lin, R. P., Martel, F., Lin, C. S., Parks, G. K., & Rème, H. (1979). Thin sheets of energetic electrons upstream from the Earth's bow shock. *Geophysical Research Letters*, 6, 401–404.
- Connerney, J. E. P., Espley, J., DiBraccio, G. A., Gruesbeck, J. R., Oliverson, R. J., Mitchell, D. L., et al. (2015). First results of the MAVEN magnetic field investigation. *Geophysical Research Letters*, 8819–8827, 42. <https://doi.org/10.1002/2015GL065366>
- Connerney, J. E. P., Espley, J., Lawton, P., Murphy, S., Odom, J., Oliverson, R., & Sheppard, D. (2015). The MAVEN magnetic field investigation. *Space Science Reviews*, 195, 257–291. <https://doi.org/10.1007/s11214-015-0169-4>
- Decker, R. B. (1983). Formation of shock-spike events at quasi-perpendicular shocks. *Journal Geophysical Research*, 88, 9959.
- Feldman, W. C., Asbridge, J. R., Bame, S. J., Gary, & Montgomery, M. D. (1975). Solar wind electrons. *Journal Geophysical Research*, 80, 4181–4196. <https://doi.org/10.1029/JA080i031p04181>
- Fitzenteiter, R. J., Scudder, J. D., & Klimas, A. J. (1990). Three-dimensional analytical model for the spatial variation of the foreshock electron distribution function: Systematics and comparisons with ISEE observations. *Journal Geophysical Research*, 95, 4155.
- Halekas, J. (2017). Structure, dynamics, and seasonal variability of the Mars-solar wind interaction: MAVEN solar wind ion analyzer in-flight performance and science results. *Journal Geophysical Research: Space Physics*, 100, 547–578. <https://doi.org/10.1002/2016JA023167>
- Halekas, J. S., Taylor, E. R., Dalton, G., Johnson, G., Curtis, D. W., McFadden, J. P., et al. (2015). The solar wind ion analyzer for MAVEN. *Space Science Review*, 195, 125–151. <https://doi.org/10.1007/s11214-013-0029-z>
- Jakosky, B. M., Lin, R. P., Grebowsky, J. M., Luhmann, J. G., Mitchell, D. F., Beutelschies, G., et al. (2015). The Mars Atmosphere and Volatile Evolution (MAVEN) Mission. *Space Science Reviews*, 195, 3–48. <https://doi.org/10.1007/s11214-015-0139-x>
- Kiraly, Y. P., Loch, K., Szegő, I., Szemerey, I. T., Szücs, M., Tatrallyay, N. M., et al. (1991). The HARP plasma experiment on-board the Phobos-2 spacecraft: Preliminary results. *Planetary and Space Science*, 39(1/2), 139–145. [https://doi.org/10.1016/0032-0633\(91\)90136-X](https://doi.org/10.1016/0032-0633(91)90136-X)
- Larson, D. E., Lin, R. P., McFadden, J. P., Ergun, R. E., Carlson, C. W., Anderson, K. A., et al. (1996). Probing the Earth's bow shock with upstream electrons. *Geophysical Research Letters*, 23(17), 2203–2206.
- Leroy, M. M., & Mangeney, A. (1984). A theory of energization of solar wind electrons by the Earth's bow shock. *Annales Geophysicae*, 2, 449–456.
- Mailing, D. H. (1992). *Coordinate systems and map projections* (2nd ed.). New York: Pergamon Press.
- Mazelle, C. X., Meziane, K., Mitchell, D. L., Garnier, P., Espley, J. R., Hamza, A. M., et al. (2018). Evidence for neutrals-foreshock electrons impact at Mars. *Geophysical Research Letters*, 45, 3768–3774. <https://doi.org/10.1002/2018GL077298>
- Meziane, K., Mazelle, C. X., Lin, R. P., LeQéau, D., Larson, D. E., Parks, G. K., & Lepping, R. P. (2001). Three-dimensional observations of gyrating ion distributions far upstream from the Earth's bow shock and their association with low-frequency waves. *Journal Geophysical Research*, 106, 5731–5742. <https://doi.org/10.1029/2000JA900079>
- Meziane, K., Mazelle, C. X., Romanelli, N., Mitchell, D. L., Espley, J. R., Connerney, J. E. P., et al. (2017). Martian electron foreshock from MAVEN observations. *Journal Geophysical Research*, 122, 1531–1541. <https://doi.org/10.1002/2016JA023282>
- Mitchell, D. L., Mazelle, C., Sauvaud, J.-A., Thocaven, J.-J., Rouzaud, J., Fedorov, A., et al. (2016). The MAVEN solar wind electron analyzer. *Space Science Review*, 200, 495–528. <https://doi.org/10.1007/s11214-015-0232-1>
- Moses, S. L., Coroniti, F. V., & Scarf, F. L. (1988). Expectations for the microphysics of the Mars-solar wind interaction. *Geophysical Research Letters*, 15, 429–432.
- Rosenbauer, H., Schwenn, R., Marsch, E., Meyer, B., Miggenrieder, H., Montgomery, M. D., et al. (1977). A survey on initial results of the Helios plasma experiment. *Journal Geophysical Research*, 42, 561–580.
- Schwartz, S. J., Thomsen, M. F., Bame, S. J., & Stansberry, J. (1988). Electron heating and the potential jump across fast mode shocks. *Journal Geophysical Research*, 93, 12923.
- Schwingschuh, K., Riedler, W., Lichtenegger, H., Yeroshenko, Y. e., Sauer, K., Luhmann, J. G., et al. (1990). Martian bow shock: Phobos observations. *Geophysical Research Letters*, 17, 889–892.
- Scudder, J. D., Mangeney, A., Lacombe, C., Harvey, C. C., & Aggson, T. L. (1986). The resolved layer of a collisionless, high β , supercritical, quasi-perpendicular shock wave, 2. Dissipative fluid electrodynamics. *Journal Geophysical Research*, 91, 11053.
- Skalsky, A., Grard, R., Kiraly, P., Klimov, S., Kopanyi, V., Schwingschuh, K., & Trotignon, J. G. (1993a). Simultaneous plasma wave and electron flux observations upstream of the Martian bow shock. *Planetary Space Science*, 41(3), 183–188.
- Skalsky, A., Grard, R., Kiraly, P., Klimov, S., Kopanyi, V., Schwingschuh, K., & Trotignon, J. G. (1993b). Simultaneous plasma wave and electron flux observations upstream of the Martian bow shock. *Planetary Space Science*, 41(3), 183–188.
- Slavin, J. A., Schwingschuh, K., Riedler, W., & Eroshenko, E. (1991). The solar wind interaction with Mars: Mariner 4, Mars 2, Mars 3, Mars 5 and Phobos 2 observations of bow shock position and shape. *Journal Geophysics Research*, 96, 11,235–11,241.
- Trotignon, J. G., Grard, R., & Klimov, S. (1991). Location of the Martian bow shock measurements by the plasma wave system on Phobos-2. *Geophysical Research Letters*, 18, 365–368.
- Vignes, D., Mazelle, C. X., Rème, H., Acuña, M. H., Connerney, J. E. P., Lin, R. P., et al. (2000). The solar wind interaction with Mars: Locations and shapes of the bow shock and the magnetic pile-up boundary from the observations of the MAG/ER experiment onboard Mars Global Surveyor. *Geophysical Research letters*, 27(1), 49–52.
- Wu, C. S. (1984). A fast Fermi process: Energetic electrons accelerated by a nearly perpendicular bow shock. *Journal Geophysical Research*, 89, 8857–62.